Relationship between the real contact area and contact force in pre-sliding regime*

Baojiang Song(宋保江) and Shaoze Yan(阎绍泽)†

State Key Laboratory of Tribology, Department of Mechanical Engineering, Tsinghua University, Beijing 100084, *China*

(Received 13 October 2016; revised manuscript received 15 December 2016; published online 6 June 2017)

The pre-sliding regime is typically neglected in the dynamic modelling of mechanical systems. However, the change in contact state caused by static friction may decrease positional accuracy and control precision. To investigate the relationship between contact status and contact force in pre-sliding friction, an optical experimental method is presented in this paper. With this method, the real contact state at the interface of a transparent material can be observed based on the total reflection principle of light by using an image processing technique. A novel setup, which includes a pair of rectangular trapezoidal blocks, is proposed to solve the challenging issue of accurately applying different tangential and normal forces to the contact interface. The improved Otsu's method is used for measurement. Through an experimental study performed on polymethyl methacrylate (PMMA), the quantity of contact asperities is proven to be the dominant factor that affects the real contact area. The relationship between the real contact area and the contact force in the pre-sliding regime is studied, and the distribution of static friction at the contact interface is qualitatively discussed. New phenomena in which the real contact area expands along with increasing static friction are identified. The aforementioned relationship is approximately linear at the contact interface under a constant normal pressure, and the distribution of friction stress decreases from the leading edge to the trailing edge.

Keywords: real contact area, contact interface, pre-sliding regime, contact force

PACS: 46.55.+d, 42.30.Va, 78.20.Ci **DOI:** 10.1088/1674-1056/26/7/074601

1. Introduction

The requirements for positional accuracy and control precision are becoming increasingly higher in the fields of mechanical engineering and aerospace. The friction between the components of a mechanical system and the nonlinear phenomena that it causes can be important factors that affect the movement and control precision of such a system. Friction analysis is an essential part of the dynamic modelling of mechanical systems.[1–3] With the development of tribology, scholars have attempted to explain the friction phenomenon between two rough surfaces by proposing models from the macroscopic and microscopic perspectives. However, these friction models are only suitable for certain occasions. To describe the peculiarities of pre-sliding friction, several scholars have studied the elastic deformation and elastic behaviour of the contact interface under tangential force, which are characterized as hysteresis with memory.[4–8] Dahl proposed the Dahl model to explain the hysteresis phenomenon in the pre-sliding regime.[9] The LuGre model introduces the average deformation of asperities to represent pre-sliding contact at the interface.[10] The Maxwell slip model regards contact asperities as a series of springs with different degrees of stiffness, which is in accord with the actual state of the contact surface.[11] To date, a consensus on the mechanism of interface friction has not yet been reached. The current study aims to visualize surface contact in the pre-sliding regime to contribute to a better understanding of pre-sliding friction.

Interconnecting micro-asperities form the real contact region between two contact surfaces. This region determines the physical properties and contact behaviour of the interface. Therefore, studying the real contact state between two rough surfaces is highly significant in determining the friction mechanism of the interface. Bowden and Tabor were the first to propose the concept of the real contact area at the contact interface.[12] Greenwood and Williamson assumed that the height distribution of micro-asperities on the surface conformed to the Gaussian distribution; they used the Hertz contact theory to solve the problem of each asperity contact individually. The introduction of the Greenwood–Williamson (GW) model has significantly affected the field of contact modelling. Since then, numerous scholars have proposed modified rough surface contact models based on the GW model.[13] Whitehouse and Archard regarded the independent contact of micro-asperities to be untenable when the load at the interface increased and deformation became larger. They believed that the curvature radius of a micro-asperity was associated with its height and proposed the WA contact model.[14] Chang *et al.* presented the CEB contact model, which considered the elastoplasticity and volume conservation of micro-asperities. The aforementioned contact mod-

*Project supported by the National Natural Science Foundation of China (Grant No. 11272171), the Natural Science Foundation of Beijing City, China (Contract No. 3172017), and the Education Ministry Doctoral Fund of China (Grant No. 20120002110070).

†Corresponding author. E-mail: yansz@mail.tsinghua.edu.cn

© 2017 Chinese Physical Society and IOP Publishing Ltd

els are all based on the assumption that the height distribution of micro-asperities is subject to the Gaussian distribution.[15] However, Majumdar and Bhushan found that the height distribution of micro-asperities was actually random and unsteady. The statistical characterization parameters of a surface acquired under certain measurement conditions could only reflect roughness information related to instrumental resolution and sampling length. These researchers introduced fractal theory to model surface contact and built the fractal contact model, which could provide roughness information at all scale ranges of rough surfaces.[16,17]

The aforementioned interface contact models are all based on certain assumptions, and theoretically estimate interface contact characteristics; therefore, the actual relationship between the interfacial force and the real contact area cannot be determined. The real contact area at the interface is difficult to obtain; thus, experimental studies on contact models remain unsystematic and insufficient compared with the adequate theoretical research on this subject. During the early 1980s, Kragelsky reported the achievements of experimental studies on the real contact state at the interface.[18] In recent decades, scholars have focused on experimental research on this area, and several methods that apply optical, electrical, and ultrasonic techniques have been used to observe the real contact state at the interface.[19,20] Furthermore, the optical method based on the total reflection principle provides additional advantages, such as intuitiveness in observing the contact state, as well as high reliability and measuring precision.[21–23]

In this paper, an optical experimental method is presented to observe the real contact state at the interface of a transparent material in the quiescent and pre-sliding regimes. This method is based on the total reflection principle of light and applies an image processing technique. The experimental setup and the principle for measuring the real contact area are introduced in Section 2. In Section 3, the main reason for the increase in the real contact area is explored, and the relationship between the real contact area and the interfacial force is determined. The distribution of static friction in pre-sliding contacts is also analysed qualitatively. The significance of the content of this paper lies in its potential to enhance knowledge of the real contact state at the interface and expand comprehension of the pre-sliding process.

2. Experiment principle

A flowchart of the experimental method is shown in Fig. 1.

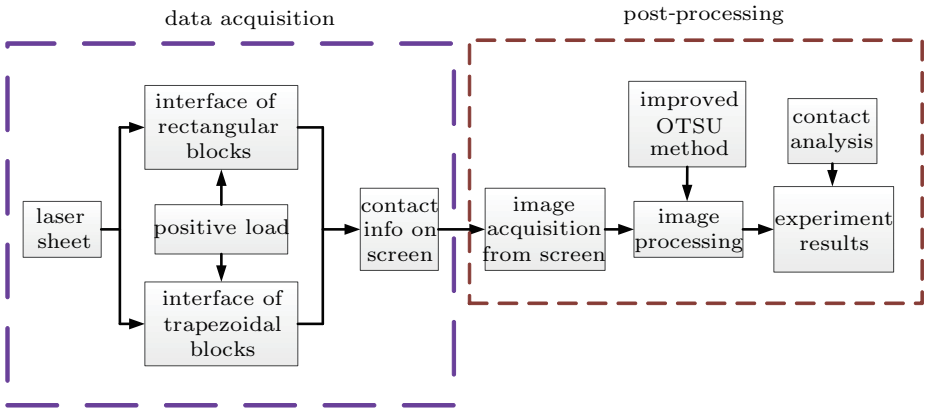


Fig. 1. (color online) Flowchart of the measuring system.

The two main steps in the measuring system are the acquisition and processing of interfacial contact data.

The schematic of the experimental setup, which presents the profile of the experimental condition, is shown in Fig. 2(a). As shown in the figure, the total reflection principle of light is applied to observe the real contact state at the interface of a transparent material, which is polymethyl methacrylate (PMMA) in this experiment. The mechanical properties of PMMA are listed in Table 1. Several interconnecting micro-asperities are found at the contact interface. These micro-asperities account for a small portion of the apparent contact area, whereas the remaining areas between the surfaces are filled with air. A red laser sheet is irradiated onto the contact interface from the lower PMMA block, as shown in Fig. 2(b). The incidence angle on the surface of the lower PMMA block should be larger than the total reflection angle of the PMMA to air, which is calculated as 42° based on the refractive index of the PMMA provided in Table 1. In the experiment, total reflection does not occur at the interconnecting micro-asperities. The incident laser sheet is divided into two parts. One part is transmitted through the interface via the interconnecting micro-asperities, whereas the other part is reflected onto the surface because of total reflection. Thus, the transmission laser produces facular points on the screen, which shows the real contact state of the contact interface.

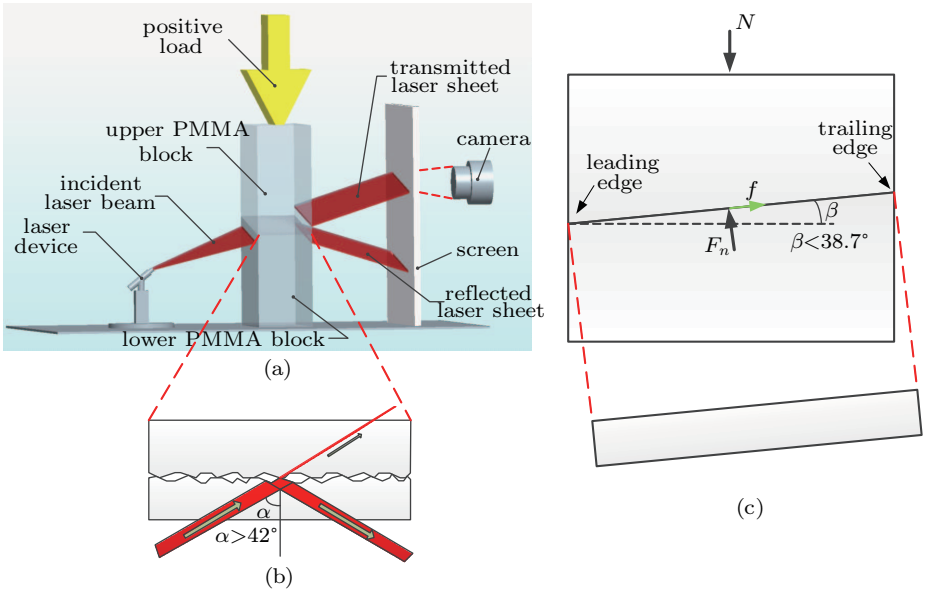


Fig. 2. (color online) Schematic of the experimental setup.

Table 1. Mechanical properties of the PMMA material.

Property	Value
Index of refraction	1.49
Tensile strength	50–77 MPa
Density	1190 kg/m^3
Transmittance	> 85%
Sa surface roughness	0.03 μm
Friction coefficient	0.8

A novel setup that involves a pair of rectangular trapezoidal blocks is proposed to address the challenging issue of accurately applying different tangential and normal forces to the contact interface. Two PMMA blocks with the same shape (i.e., rectangular trapezoidal) are used as experimental samples. The two blocks are stacked together, as shown in Fig. 2(c). The top surface of the upper block is in a horizontal direction, and β is the angle between the contact interface and the horizontal plane, which is smaller than the self-lock angle of the PMMA material, $\beta < \arctan 0.8 = 38.7^\circ$ (according to the friction coefficient given in Table 1). In the experiment, the lower PMMA block is fixed to the foundation support, whereas the upper block is regarded as a sliding block. The vertical load is provided by an electronic universal testing machine (EUTM) placed uniformly on the top surface of the experimental samples. The EUTM can provide pressure ranging from 0 N to 20 kN at a constant loading rate in the vertical direction. During loading, the experimental samples remain in a static state from the macroscopic viewpoint. The contact interface of the samples exhibits pre-sliding friction from the perspective of the interconnecting micro-asperities at the interface. The loading analysis of the upper block is performed as depicted in Fig. 2(c).

$$\begin{cases} F_n = N\cos\beta, \\ f = N\sin\beta, \end{cases} \tag{1}$$

where N is the vertical pressure from the top, F_n is the supporting force from the lower PMMA block, and f is the static friction at the interface. The vertical force data can be recorded completely with the EUTM; thus, both the normal force and the tangential static friction at the contact interface can be calculated using Eq. (1) at any period during the experiment. However, for a certain set of experiments, both the normal force and the tangential force change with the vertical loading force; therefore, the control variable method cannot be conducted for one set of experiments. To address this issue, four groups of test samples at different β angles (0°, 6°, 9°, and 12°) are provided in the experiment process. In this manner, variations in the real contact area with different static friction values under a certain normal pressure can be obtained. Moreover, the relationship between the real contact area and normal pressure under a certain tangential force can be determined. All the experiments are performed in a darkroom; other details of the experimental setup and conditions have been described elsewhere.[23] Notably, the loading device should be suspended when acquiring the contact image to eliminate the hysteresis effects caused by the inner friction of the PMMA.

As shown in Fig. 3, a digital single-lens reflex (DSLR) camera is used to record the changing process of the contact state during loading when $\beta = 0^\circ$. The red area in the image is formed by the red laser, which transmits through the interconnecting micro-asperities, whereas the dark area is attributed to the laser beam reflected onto the surface of the lower PMMA block. Therefore, the red spots on the images represent the real contact area at the interface. The dark area evidently decreases with the increase in normal pressure during loading as shown in Fig. 3. The red pixels on the image are selected and combined, and the proportion of the real contact area to the apparent contact area can be determined. To select the red

pixels on the image, an improved Otsu's method (an image segmentation technique mentioned in Ref. [23]), which considers both the whole image and the local details of the photo, is applied during image processing.[23,24] The relationship between the real contact area and the contact force in the pre-sliding regime is obtained through image processing and an analysis of the experimental results.

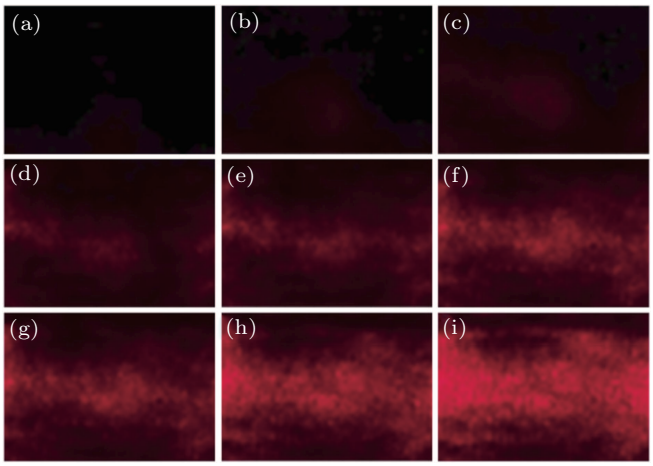


Fig. 3. (color online) Images taken by the DSLR during the loading process.

3. Preliminary experimental results and discussion

A series of experiments were conducted using the experimental method mentioned earlier on different test samples at $\beta = 0°$, $6°$, $9°$, and $12°$. The changes in the real contact area and the interfacial force were recorded in each experiment set. The experimental results and the analysis process are presented in this section.

3.1. Real contact area and normal pressure

The relationship between the real contact area and normal pressure was simulated as a linear correlation using the rough surface contact models mentioned in Section 1. This approach is used regardless of whether the rough surface is assumed a Gaussian distribution surface or a fractal surface.

However, the relationship between the real contact area and normal pressure is not linear based on the results of the experimental study on measuring the real contact area using PMMA. Figure 4 shows the relationship between normal pressure and the normalized contact area at the interface. As shown in the figure, the transmitted laser cannot effectively form a bright spot on the screen when normal pressure is within the range of 0–0.33 MPa. Thus, a dead zone is observed while measuring the real contact area using the optical method based on the total reflection principle. When normal pressure is within the range of 0.33–1.28 MPa, the real contact area linearly increases with the increase in normal pressure. When normal pressure exceeds 1.28 MPa, the real contact area expands, whereas its growth rate decreases with increasing normal pressure.

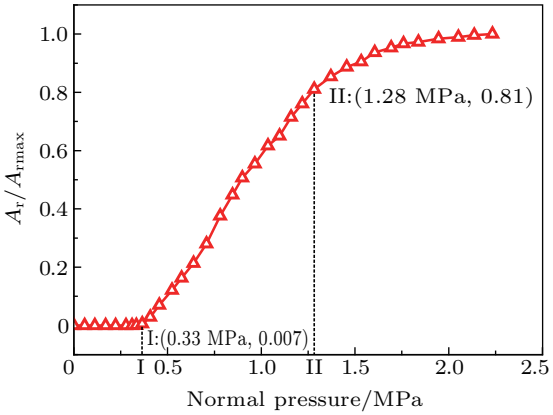


Fig. 4. (color online) Real contact area versus normal pressure during loading.

An analysis of the experiment phenomena explains why the optical method does not work under low normal pressure. The actual surface profile of the experimental sample measured using a white light interferometer is provided in Fig. 5(a). As shown in the figure, a small fraction of peaky asperities with a higher altitude of over 80 nm above the zero line exists on the surface and occupies less than 1% of the total number of micro-asperities. Higher asperities enter the contact state first when normal pressure is lower at the contact interface. However, the contact spot diameter of the asperities with a higher altitude has a magnitude equal to the wavelength of the red laser (550 nm). Thus, diffraction phenomena occur at the contact spot when the transmitted laser reaches the contact spot at the interface and, consequently, severely weaken the illuminance of the transmitted laser. Diffracted rays from different contact spots were interlaced and projected onto the screen; therefore, the real contact state at the interface could not appear effectively on the screen. With the increase in normal pressure, the first batch of asperities participating in surface contact underwent deformation, and the area of the contact spot increased with the expansion of the diameter. As deformation at the interface increased, more micro-asperities with a lower altitude participated in surface contact, thereby forming a larger bearing surface. The diffraction phenomenon was reduced as the contact area at each contact spot expanded, and the transmitted laser effectively formed light spots on the screen.

The contact process of the sample interface under different normal pressure values can be divided into three stages according to the curves depicting the relationship between normal pressure and the normalized contact area in Fig. 4, and the analysis content based on Fig. 5. When normal pressure is within the range of 0–0.33 MPa, a few higher asperities

form small contact spots at the interface. During this interval, the carrying capacity of the interconnecting micro-asperities is weak. If a tangential force is applied to the contact interface, then tangential deformation will easily occur at higher contact asperities. Shear failure and wear will also occur, with the shear stress exceeding the shear strength of the material. When normal pressure ranges from 0.33 MPa to 1.28 MPa, the quantity of the asperities participating in contact rapidly increases, thereby leading to the rapid growth of the real contact area. During this interval, the relationship between the real contact area and normal pressure is linear. The increasing quantity of the interconnecting asperities is proven to be the main cause of the extension of the real contact area. Once normal pressure exceeds 1.28 MPa, the addition of interconnecting asperities becomes slower with increasing normal pressure, and the growth rate of the real contact area also decreases. The main bearing area is formed during this interval.

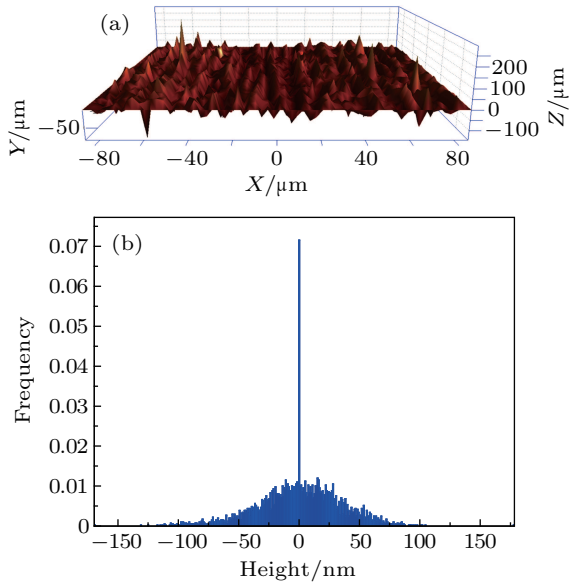


Fig. 5. (color online) Actual surface profile measured using a white light interferometer and the altitude distribution of the asperities on the surface.

3.2. Real contact area and static friction

To investigate the relationship between the real contact area and static friction in the pre-sliding regime, vertical loading experiments were conducted using four groups of test samples at different β angles (0°, 6°, 9°, and 12°). The loading force was recorded, and the vertical force was decomposed into two directions: perpendicular and parallel to the contact interface. Thus, the relationship between the real contact area and static friction could be determined. The relation curves of normal pressure and the normalized contact area at different β angles are shown in Fig. 6.

As shown in the figure, the real contact area of the interface increases with the increase in the β angle. As mentioned in Section 2, when the normal pressure values at the interface at different β angles are the same, the system with the larger β angle exhibits a higher static friction. The experimental study on pre-sliding contacts showed that the real contact area expands with the increase in static friction under a constant normal pressure.

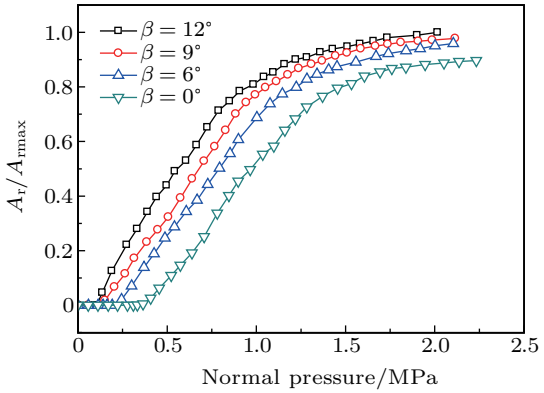


Fig. 6. (color online) The relationship between real contact area and normal pressure at different β angles.

Figure 7 presents the relation curves of the normalized contact area and static friction under six constant normal pressure levels. As shown in the figure, the relationship between the real contact area and static friction is similar to the linear correlation under a constant normal pressure and maximum load in the experiment. In addition, the influence on the change process of the real contact area caused by static friction decreases with increasing normal pressure at the interface.

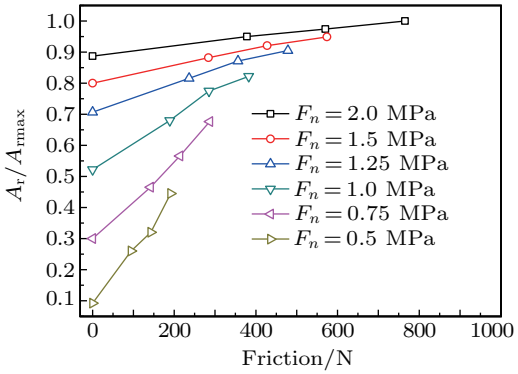


Fig. 7. (color online) Real contact area vs. static friction under different normal pressure levels.

3.3. Distribution of friction stress at the interface in the pre-sliding regime

The distribution of static friction stress at the interface was determined qualitatively in pre-sliding friction through the observation and analysis of the contact images obtained in the experiments. Figure 8 shows the contact images, which represent the distribution of transmission light with the increase of contact force at the β angle of 9°.

As shown in the figure, the light intensity of the transmitted laser decreases gradually along the direction of the interface from the leading edge to the trailing edge during each

loading stage. The distribution of light intensity on the screen indicates that the distribution of the real contact area at the interface also decreases from the leading edge to the trailing edge in pre-sliding contacts. The same experimental phenomenon was also observed at $\beta = 6^\circ$ and 12°.

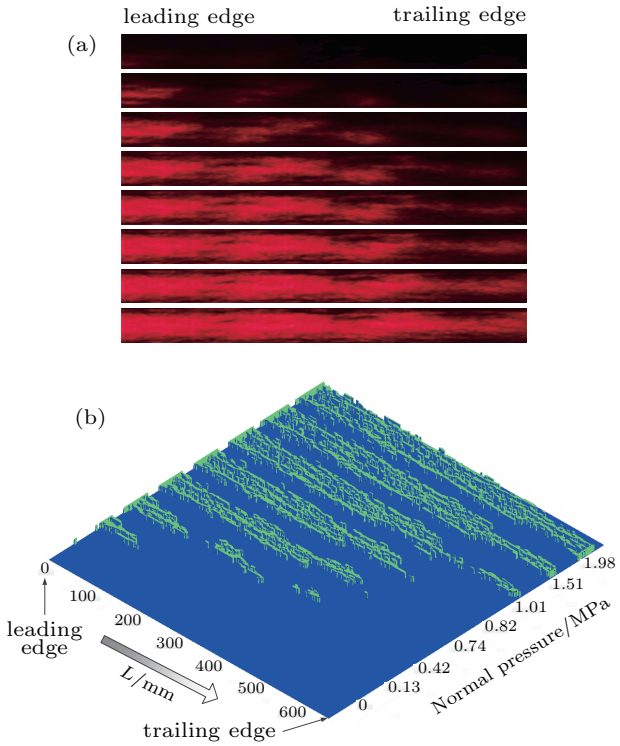


Fig. 8. (color online) Distribution of real contact points at the interface at $\beta = 9^\circ$.

Normal stress is uniform at each position of the contact interface during loading; hence, the non-uniformity of friction stress leads to a decrease in the real contact area from the leading edge to the trailing edge. As mentioned in Section 3.2, the real contact area increases with the increase in static friction, and thus, a conclusion can be drawn that the distribution of friction stress decreases from the leading edge to the trailing edge.

4. Conclusion

In this study, the relationship between the real contact area and the interfacial force at the contact interface of a transparent material in the pre-sliding regime was studied based on the principle of total reflection and the improved Otsu's method through a series of experiments. The real contact state at the interface was observed intuitively using an optical method. A tangential load was applied to the contact interface in a quasi-static state, and the magnitude of the static friction was obtained accurately in the experimental study.

Several conclusions can be drawn from the analysis of the experiment principle and the experiment results.

(i) The diffraction phenomena at the small contact spot formed by higher asperities explain why the optical method does not work under low normal pressure.

(ii) The increasing quantity of the interconnecting asperities was proven to be the dominant factor that expands the real contact area.

(iii) The real contact area expands with the increase in static friction under a constant normal pressure with an approximately linear relationship in the pre-sliding regime, and the influence on the change process of the real contact area caused by static friction decreases with increasing normal pressure.

(iv) The distribution of friction stress decreases from the leading edge to the trailing edge in pre-sliding contact.

The real contact area is a random quantity that changes within a certain range; hence, the normalized contact area was used in this study. In addition, experimental studies on the real contact state of the contact interface should focus more on its properties and phenomena rather than on the exact value of the real contact area.

References

[1] Yang T F, Yan S Z and Han Z Y 2015 *J. Sound. Vib.* **341** 246
[2] Xiang W W K, Yan S Z and Wu J N 2015 *Sci. China Technol. Sc.* **58** 86
[3] Ma D H, Wu J N and Yan S Z 2016 *Sci. China Technol. Sc.* **59** 1305
[4] Johnson K L 1955 *P. Roy. Soc. A-Math. Phys.* **230** 531
[5] Courtney-Pratt J S and Eisner E 1957 *P. Roy. Soc. A-Math. Phys.* **238** 529
[6] Ishigaki H, Kawaguchi I and Mizuta S 1979 *Wear* **54** 157
[7] Futami S, Furutani A and Yoshida S 1990 *Nanotechnology* **1** 31
[8] Otsuka J 1992 *Nanotechnology* **3** 29
[9] Dahl P R 1968 *A Solid Friction Model* (AEROSPACE CORP. EL. SEGUNDO. CA.)
[10] Canudas D W C, Olsson H, Astrom K J and Lischinsky P 1995 *IEEE. T. Automat. Contr.* **40** 419
[11] Rizos D and Fassois S 2005 *European Control Conference*, December 12–15, 2005, Seville, Spain, p. 4578
[12] Bowden F P and Tabor D 1950 *The Friction and Lubrication of Solids* (London: Oxford University Press) p. 1
[13] Greenwood J A and Williamson J B P 1966 *Proc. R. Soc. Lond. A* **295** 300
[14] Whitehouse D J and Archard J F 1970 *Proc. R. Soc. Lond. A* **316** 97
[15] Chang W R, Etsion I and Bogy D B 1987 *J. Tribol.* **109** 257
[16] Majumdar A and Bhushan B 1990 *J. Tribol.* **112** 205
[17] Majumdar A and Bhushan B 1991 *J. Tribol.* **113** 1
[18] Kragelsky I V and Alisin V V 1981 *Firction, Wear, Lubircation-Tribology and Book* (Moscow: Mir Publishers) p. 425
[19] Eguchi M, Shibamiya T and Yamamoto T 2009 *Tribol. Int.* **42** 1781
[20] Tuononen A J 2014 *Tribol. Int.* **69** 70
[21] Ben-David O, Rubinstein S M and Fineberg J 2010 *Nature* **463** 76
[22] Ben-David O, Cohen G and Fineberg J 2010 *Science* **330** 211
[23] Song B J, Yan S Z and Xiang W W K 2015 *Chin. Phys. B* **24** 014601
[24] Otsu N 1975 *Automatica* **11** 23